Characterization of the 46.9-nm soft X-ray laser beam from a capillary discharge

S. Barnwal · Y. B. S. R. Prasad · S. Nigam · K. Aneesh ·
M. L. Sharma · R. P. Kushwaha · P. K. Tripathi · P. A. Naik ·
J. A. Chakera · C. P. Navathe · P. D. Gupta

Abstract Intense lasing had been obtained from argon plasma in the soft X-ray region from a capillary discharge plasma system. Different diagnostics have been used to characterize the lasing properties by recording the temporal, spatial, and spectral profiles of the emission. The divergence measurement indicates that the soft X-ray laser beam has good directionality with a divergence of 3.5 mrad. The spectrum of the laser beam measured using a transmission grating showed intense lasing line at 46.9 nm. Diffraction orders as high as 10th orders were observed. The temporal profile recorded with a vacuum diode showed a distinct laser peak with a pulse width $\sim$1.2 ns (FWHM). In addition, the coherence of the X-ray laser beam was also confirmed from the high-contrast interference fringes (visibility $\sim$85 %) recorded using double slits.

1 Introduction

The quest for obtaining lasing action in the shorter wavelengths started right from the invention of laser in 1960. The research in the soft X-ray lasers is currently driven by a wide range of potential applications such as nano-imaging [1], X-ray holography [2], lithography [3], dense plasma diagnostics [4]. Efforts have been made in the past and are still going on in various laboratories [5–14] worldwide to build X-ray lasers using different techniques, e.g., laser-produced plasmas at high laser intensities [6–

10], high-order harmonics generation (HHG) from laser-produced plasmas with fs lasers [11], X-ray free-electron lasers [12], and capillary discharge plasmas [13, 14]. All these approaches are complimentary to each other in their advantages and limitations. The X-ray lasers produced from laser-produced plasmas have the advantage of short pulse duration but suffer from smaller gain volume, resulting in lower flux and no tunability, although they can be generated at a variety of wavelengths by changing the lasing element. High-order harmonics are partially tunable and offer high brightness but have low conversion efficiency. The free-electron lasers (FEL) have two important advantages of broad tunability and high average power. However, they are expensive to construct. Some mixed approaches were also implemented to exploit the advantages of different approaches, like using high-order harmonics as a seed pulse to get good optical quality and amplifying them in laser-driven plasma amplifier, resulting in energetic soft X-ray laser pulses [15, 16]. On the other hand, fast electric discharge in a gas-filled capillary provides a promising alternative to the aforesaid schemes of making soft X-ray laser. This technique has several advantages [13] over other schemes, such as high efficiency for producing multiply ionized hot and dense plasma column with a large aspect ratio ($\sim$1,000:1) with high uniformity, capability to deliver higher photon flux in the lasing wavelength, and relatively compact size compared to big facilities such as FELs or high-power laser systems.

The X-ray laser research through capillary discharge approach was intensified after the first observation of amplification in the $3s\,^1P_1$–$3p\,^1S_0$ transitions of Ne-like Ar^{8+} ions by Rocca et al. [14] and demonstration of a tabletop soft X-ray amplifier in saturated region [17, 18]. Here, the lasing was achieved via collisional excitation of

S. Barnwal (✉) · Y. B. S. R. Prasad · S. Nigam · K. Aneesh ·
M. L. Sharma · R. P. Kushwaha · P. K. Tripathi ·
P. A. Naik · J. A. Chakera · C. P. Navathe · P. D. Gupta
Raja Ramanna Centre for Advanced Technology,
Indore 452013, M.P., India
e-mail: sbarnwal@rrcat.gov.in

Ne-like Ar ions generated by a fast capillary discharge. Achieving soft X-ray lasing through capillary discharge is not an easy task due to various complexities involved therein. This can be seen from the fact that after the first demonstration by Rocca et al., no other group could reproduce these results for next 6–7 years. Ben-kish et al. [19], from Israel, were successful in demonstrating soft X-ray lasing in argon and emphasizing the role of pre-ionization in lasing. After this, groups from Japan [20–24], Italy [25–28], Malaysia [29, 30], China [31–34], and Czech Republic [35] have also reported successful demonstration of soft X-ray lasing in argon plasma on different experimental configurations. We, at Raja Ramanna Centre for Advanced Technology (RRCAT), India, had also started this activity few years back and recently confirmed lasing action using multiple measurements which include temporal, spatial, and spectral characterization of the X-ray laser and measurements of the coherence length. We are reporting these results in the present paper.

The outlay of the paper is as follows. In Sect. 2, the capillary discharge X-ray laser scheme has been discussed briefly. The following section covers the experimental setup and optimization of the conditions leading to observation of lasing. We also discuss about the electro-magnetic interference (EMI) and precautions taken to reduce this like using Faraday cage, doubly shielded cables, isolation transformers, etc. The results obtained from different experimental studies are discussed in Sect. 4. We would like to draw attention on a few points here. We have recorded intense lasing line of argon capillary discharge X-ray laser using a transmission grating spectrograph (TGS), showing various higher diffraction orders of the lasing line, which has not been reported in the literature so far. By modifying the distances involved in the TGS, diffraction orders as high as 10th could be recorded. Recording of such a high diffraction order is normally difficult due to very small energy being coupled into it. The advantage with higher diffraction orders is that the accuracy of measuring the wavelength of a line in the spectrum gets enhanced 'n' times for nth diffraction order.

2 Capillary discharge X-ray laser scheme

In this scheme, electrical energy is pumped into a gas filled in a capillary by passing a fast-rising current pulse ($dI/dt > 10^{11}$ A/s) which has a large amplitude ($\sim$ few tens of kA) and fast rise time (few tens of ns). Building a pulsed power system by delivering such a fast as well as high current is by itself a challenging task. Usually, in order to generate current pulse with a fast rise time, a waterline capacitor is charged up to few hundreds of

kilovolts using a Marx bank and then discharged through the gas column using a fast switch (usually a pressurized spark gap). It is experimentally seen that in order to get reliable lasing action, it is better to pass the main discharge current through a pre-ionized gas rather than neutral gas. It is seen that this minimizes the occurrences of plasma instabilities. The pre-ionization is achieved by passing a 10–50 A current pulse a few μs before the main current. Since the pre-formed plasma has very high conductivity, the main current flows through a thin outer layer (within skin depth) of the plasma column. The high discharge current generates a magnetic field in the azimuthal direction, and the resulting radial $J \times B$ force pushes the plasma column radially inward, i.e., from the wall toward the axis. A high value of 'dI/dt' helps in fast detachment of this plasma column from the wall of the capillary, thereby minimizing the impurities from the wall in the gas plasma. During the radial compression (pinching) of the plasma column, the temperature and ionization of the plasma column significantly increase due to enhanced collisions between the electrons and the ions. As a result, a highly ionized, hot, dense plasma column is formed (Z—pinch). As the compression progresses, the density and the temperature of the plasma increase, and at one time, the kinetic pressure (nkT) acting in the radially outward direction becomes equal to the Lorentz force acting in the radially inward direction, known as the Bennett's equilibrium condition [36–38]. The pre-ionization helps in achieving a high axial uniformity and a large length to diameter aspect ratio of the order of 1,000:1 in the plasma column. Optimization of the different experimental parameters is required to achieve a high abundance of Ne-like argon ions (the lasing species) in the plasma and also for achieving population inversion between the appropriate lasing levels populated through collisional excitation by the plasma electrons. A strong amplification has been shown for the 3 s $^1P_1$–3p $^1S_0$ transition at 46.9 nm in the argon plasma by various groups worldwide, as mentioned previously [18–35]. The hot, dense plasma column lasts for a very short duration (order of ns) after which it expands outwardly toward the capillary wall. This occurs due to the radially outward kinetic pressure, in absence of the radial compression due to the Lorentz force once the current pulse is over. The efficient pinching of plasma column depends on various parameters such as pre-plasma conditions, discharge current, gas pressure in the capillary. For achieving strong amplification in Ne-like Ar^{8+} species requiring higher abundance of Ar^{8+} ions, optimum conditions like electron density $\sim 10^{18-19}$ cm^{-3}, and temperatures in the range of 60–80 eV are needed, in addition to a suitable electron density profile and a small transverse dimension of the plasma column [39, 40].
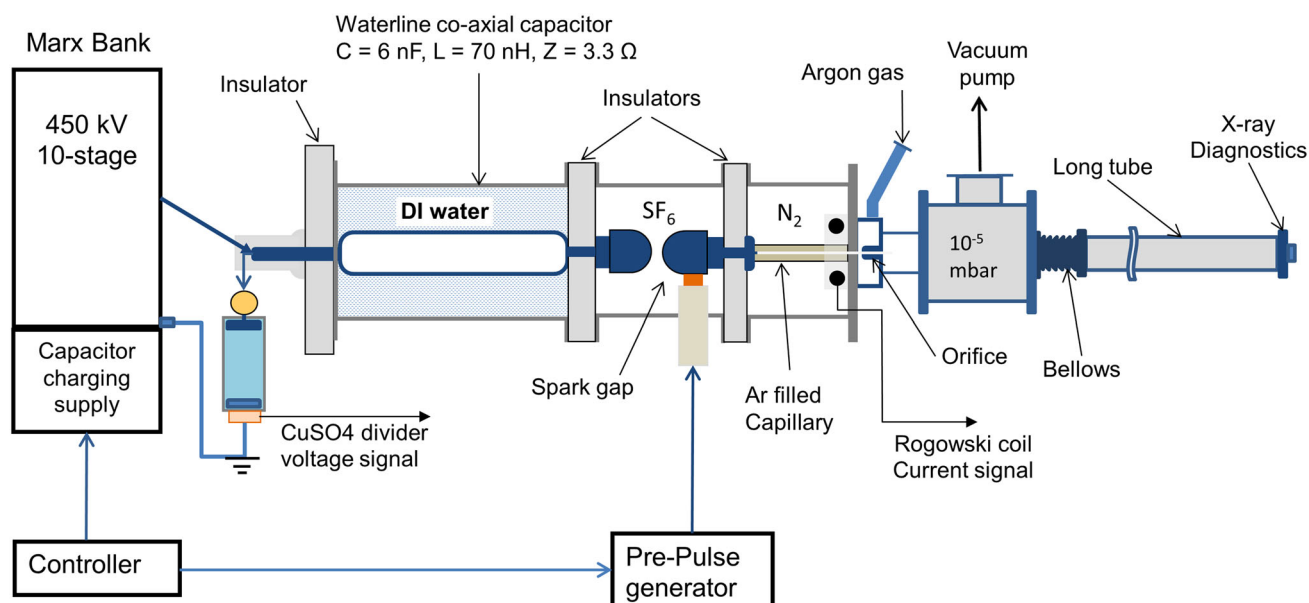
Fig. 1 A schematic diagram of the capillary discharge system

3 Experimental details

Experiments were carried out to obtain soft X-ray lasing from argon plasma in the capillary discharge X-ray laser system developed at RRCAT. A schematic diagram of the system is shown in Fig. 1, and a photograph of the actual system is shown in Fig. 2. The details of the capillary discharge X-ray laser system are reported elsewhere [41]. However, for the sake of completion, a brief description of the system is given here. In order to get a fast current pulse, a 450 kV ten-stage Marx generator was erected up to a voltage of ~ 300 kV, to charge a pulse forming line (PFL) in the form of a coaxial waterline capacitor ($C = 6$ nF, $L = 70$ nH and $Z = 3.3$ Ω) consisting of two coaxial 60-cm-long cylinders. The inner radius of the outer cylinder was 26.6 cm, and the outer radius of the inner cylinder was 16.8 cm. The space between these two cylinders was filled with low-conductivity deionized water (conductivity <2 μS) due to its large dielectric constant (80) which results in low leakage current and high breakdown strength. The PFL was discharged through a self-triggered spark gap pressurized by SF_6 gas. The spark gap acts as a fast switch to drive a fast current into the gas column inside a capillary. The breakdown voltage was adjusted by varying the distance between the electrodes and the gas pressure. SF_6 gas was chosen as filler gas due to its high breakdown strength (~ 3 times higher than that of air). A typical voltage pulse from the Marx bank is of few μs duration. Using a combination of a fast capacitor and a spark gap, one gets a current pulse with rise time of few tens of ns. A pre-pulse generator provides a

suitable pre-pulse current required for creating low-temperature plasma before the main discharge. The pre-pulse is applied through a $CuSO_4$ solution-based resistor in contact with the spark gap electrode on the capillary side. This current can be varied by adjusting the resistance by varying the concentration of the $CuSO_4$ solution. This current pre-pulse (15–40 A) was applied few microseconds (5–10 μs) before the main pulse to obtain uniform pre-ionization in the capillary.

The operations of charging and triggering of the Marx bank and the pre-pulse generator are controlled by a microcontroller-based system. Using this controller, one can also adjust the delay between the pre-pulse and the main voltage pulse (Marx bank). The control system also gets feedback from the Marx bank voltage pulse. More details of the control system are reported elsewhere [42]. The peak current of the main discharge can be varied by controlling the erected voltage on the PFL and pressure of the SF_6 gas in the spark gap. This current then passes through an argon gas filled in a ceramic (alumina) capillary of 15 cm length and 2.8 mm diameter.

For the electrical discharge in the capillary, the PFL side electrode acts as the high-voltage electrode and a 1-mm tungsten orifice located near the other end of the capillary acts as the ground electrode. This orifice also helps in maintaining a differential pressure. There is a small-volume (~ 40 cm^3) 'argon chamber' in between the capillary and the orifice as shown in Fig. 1. In our initial setup, there was an additional ground electrode right on the end face of capillary in addition to this orifice. In this configuration,

Fig. 2 A photographic view of the capillary discharge system
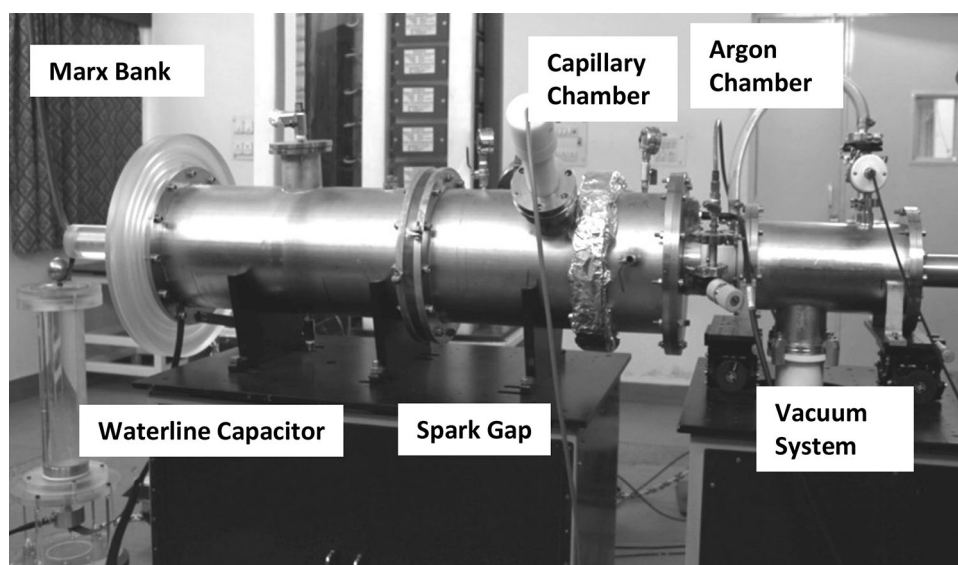
there was a problem due to the presence of cold argon between the ground electrode and orifice which can strongly attenuate the generated soft X-ray signal. Hence, the argon chamber was designed so as to minimize the distance between the ground electrode and the orifice (2–3 mm) to minimize the length of this cold argon. Later on, the ground electrode, placed on the capillary end face, was also removed, and now, the orifice itself acts as the ground electrode. In this configuration, the problem of absorption of soft X-rays by cold argon is practically eliminated. The argon gas is filled through a fine gas-dosing and regulating valve (Pfeiffer EVN-116) into the argon chamber. In order to minimize the pressure gradients across the long capillary, two measures are taken. First, by closing the dosing valve, the argon chamber and the capillary are evacuated to 10^{-3} mbar pressure after each shot. Then, argon gas is filled to the required pressure. Before taking next shot, 1–2 min time interval is spent to stabilize the distribution of the argon gas inside the capillary. As measuring the pressure distribution inside the capillary is not possible due to the closed geometry of the capillary, the pressure in the argon chamber was measured and controlled. Vacuum is achieved on the other side of the orifice (diagnostic side) using a turbo-molecular pump (TMP) backed by a rotary pump. This orifice is responsible for maintaining a differential pressure between the argon gas chamber and the diagnostic side, which has to be maintained below 10^{-4} mbar for reducing the absorption of the soft X-rays. Depending on the requirement, the argon gas pressure in the capillary could be varied continuously (0.1–0.7 mbar) by adjusting the inlet gas pressure through the fine gas-dosing valve.

The discharge current was monitored using a calibrated Rogowski coil placed around the ceramic capillary near the ground electrode. The high voltage was monitored at the Marx generator output stage using a $CuSO_4$ voltage divider. The radiation emitted from the plasma was characterized in the temporal domain using a vacuum diode and a quadrant vacuum diode. The signal was monitored on a digital oscilloscope (Lecroy: 1 GHz, 10 GS/s). The radiation was also characterized in the spectral domain using a TGS, consisting of a 700 lpm transmission grating followed by micro-channel plate (MCP). The MCP output was imaged on a charge-coupled detector (CCD). Since the vacuum around MCP must be better than 10^{-5} mbar, another TMP was used near the MCP. During the discharge of the Marx bank, significant EMI is generated, which interferes with the control system, various diagnostics, and measuring instruments, and hence, it needs to be suppressed. For this purpose, all the measuring instruments and control systems were kept inside an EMI-shielded Faraday cage. Special double-shielded cables were used to carry electrical signals to the Faraday cage in order to minimize the EMI coupling into the signal. Grounding for the pulse power system and the control systems was separated to avoid any electrical pickup through line voltage. Isolation transformers were used wherever isolation of the instrument from electrical noise was required. In addition, all the control signals are passed through optical fibers to minimize the EMI coupling.

4 Results and discussion

The X-ray lasing in the capillary discharge depends on various experimental parameters such as discharge current, its half-cycle duration, amplitude and temporal profile of the pre-pulse, delay between the pre-pulse and main
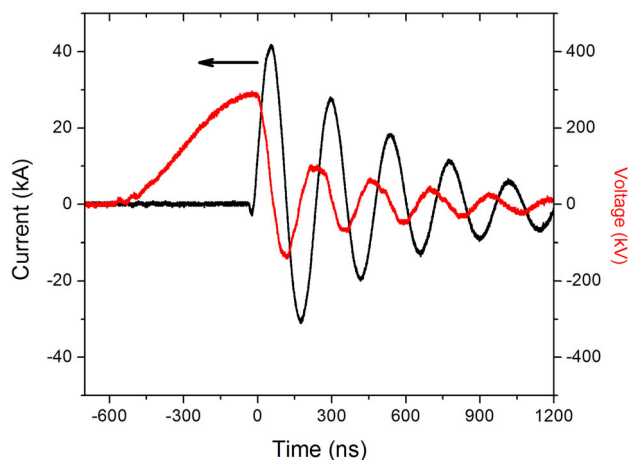
Fig. 3 Voltage and current waveforms of the main discharge in the capillary
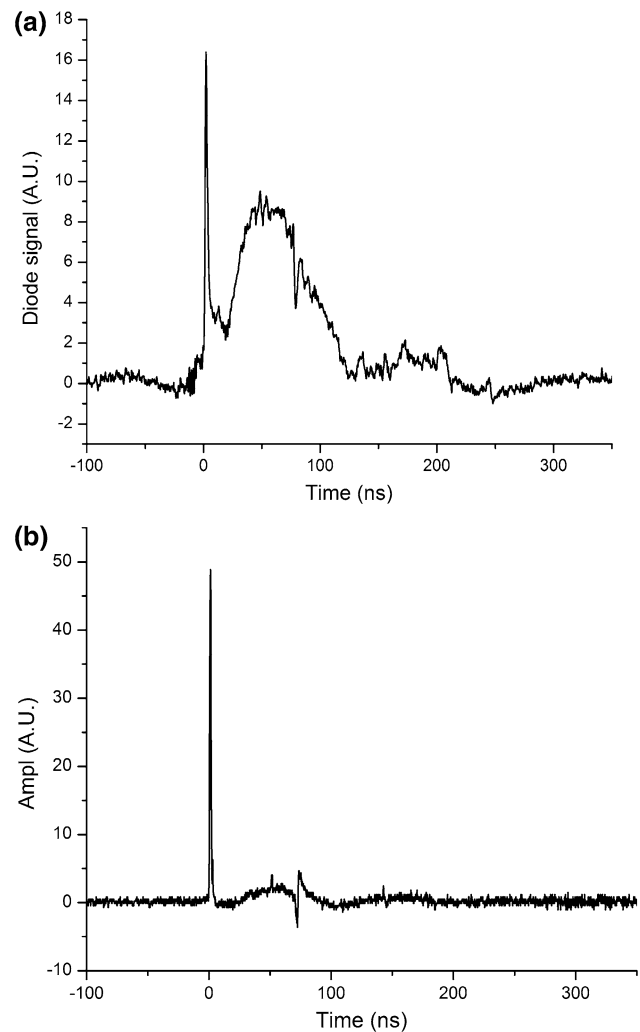

Fig. 4 Vacuum diode signals **a** showing the two types of X-ray emissions at a distance of 83 cm from the source, and **b** same signal at a larger distance (1.7 m), showing the dominance of the lasing signal

discharge currents, and the initial argon gas pressure in the capillary. All these parameters control the final temperature, density, and dimensions of the pinched plasma column, which finally leads to the X-ray lasing. Initially, a discharge current of 26 kA was passed through the Ar-filled capillary. Argon pressure in the capillary was continuously varied in the range from 0.1 to 0.7 mbar to get the lasing condition. Pre-pulse was also tuned in the range 10–25 A and was applied about 5 μs before the main pulse. Figure 3 shows a recorded typical current and voltage profiles of the main discharge in the capillary. One can see that as the main spark gap breaks down, the voltage falls sharply and the discharge current begins to rise rapidly. Both the voltage and the current waveforms have oscillations due to under-damped discharge circuits. Use of double-shielded cables to carry voltage and current signal up to the oscilloscope inside the Faraday cage significantly improved the voltage and current waveforms which are otherwise quite noisy due to EMI.

The temporal profile of the emission from capillary was recorded by a vacuum diode with a large sensor of 30 mm diameter. This diode has a copper cathode and a stainless steel mesh acting as the anode, placed at a separation of 1 mm from the cathode. The diode is reverse biased by applying a bias voltage of 0.7 kV across its electrodes. A typical signal recorded by the vacuum diode under optimization, at a distance of 83 cm from the source, is shown in the Fig. 4a. In the first half-cycle of the current, the temporal profile of the vacuum diode signal shows the presence of two distinct types of X-ray emissions from the plasma. When the diode is placed 50–100 cm away from the capillary, a relatively long-duration radiation pulse (FWHM ∼50 ns) is seen which starts ∼10 ns after the initiation of discharge current and peaks after ∼80–90 ns. This broad pulse corresponds to the bremsstrahlung

emission from the hot plasma column. Superimposed on this broad pulse, another short-duration X-ray pulse is also recorded before the peak of the current pulse. This pulse lasts for comparatively much shorter duration for few ns and corresponds to the emission from plasma during the final phase of the pinching process. It is observed that the rise time of the short-duration pulse is quite sensitive to the pressure of the argon gas in the capillary. By monitoring this rising edge, the gas pressure in the capillary was varied in fine steps, till a fast-rising signal with a rise time (10–90 % of the amplitude) of 1–2 ns was observed, as shown in Fig. 4a. The falling edge of this fast signal is not clearly visible in the recorded time profile due to the contribution from the background X-ray radiation from plasma. Therefore, the vacuum diode was moved away from the capillary end. A typical signal recorded at a distance of 1.7 m from the capillary is shown in Fig. 4b. By doing so,
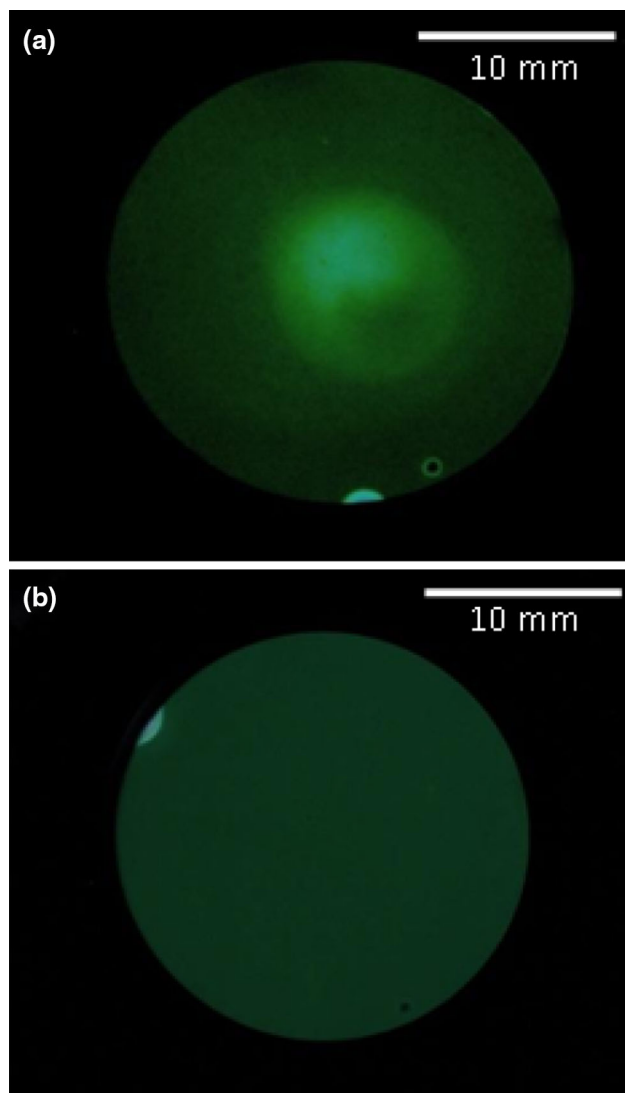
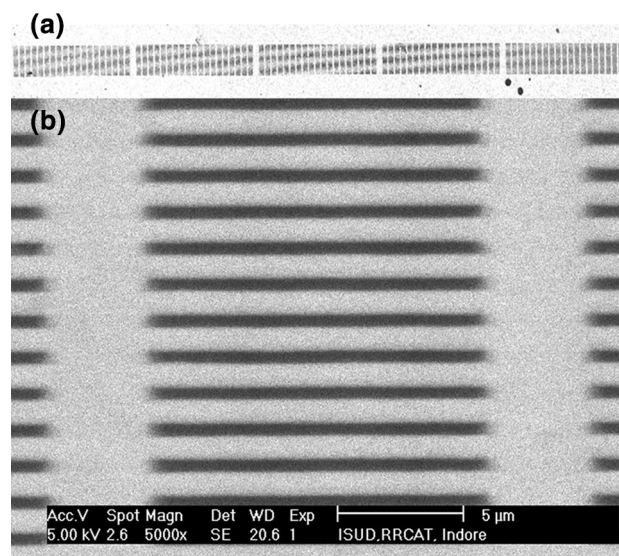Fig. 5 Spatial profile recorded on the MCP **a** with pre-pulse and **b** without pre-pulse

Fig. 6 SEM image of **a** the transmission grating with its entire slit visible and **b** a magnified image of the grating bars

the high divergence background radiation is selectively reduced with respect to the fast rise signal which indicates that this fast rise signal has good directionality compared to the background radiation. Also, this fast signal with measured pulse duration of ~ 1.2 ns (FWHM) appears only in presence of the pre-pulse. Later on, we show that this fast signal indeed corresponds to lasing in the argon plasma. In order to enhance the amplitude of this pulse, the discharge current was increased in steps and the various experimental parameters were also optimized at each step. Most optimum condition was found at a discharge current of 40 kA with rise time of 50–60 ns, Ar gas pressure of 0.35 mbar, pre-pulse current of ~ 20 A, passing 5 µs before the main current pulse, and the vacuum diode placed at a distance of 1.7 m from the capillary.

In order to measure the divergence of the X-ray beam, the spatial profile of the beam was recorded at a 1.7 m from source, on a MCP detector whose phosphor screen was imaged on to a CCD camera. The spatial profile (Fig. 5) clearly shows an intense low divergence beam superimposed over the highly divergent plasma radiation filling the entire MCP screen. The divergence of the beam was estimated to be <3.5 mrad. This low divergence beam appears only when both the pre-pulse and main current are present. It may be recalled that the fast signal in the vacuum diode also disappears when there is no pre-pulse. This clearly establishes the lasing characteristics of this beam. In the absence of pre-pulse, only the incoherent plasma emission is seen on the MCP screen as shown in Fig. 5b. The small bright spot partially visible on the MCP edge in the images (Fig. 5a, b) is artifacts due to unwanted discharge occurring on the MCP during the shot (defects).

In order to determine the lasing wavelength, the spectrum of the emitted radiation from the capillary was recorded under optimum condition described above. For this purpose, a free-standing gold transmission grating having 700 lpm with a 100 µm slit (oriented perpendicular to the dispersion plane) was used. The SEM image of this transmission grating along with its slit is shown in Fig. 6a, and the magnified image of the grating bars is shown in Fig. 6b.

The position of the grating was precisely matched with the center of the X-ray laser beam to get maximum intensity in the transmitted spectrum. This was done with the help of a quadrant vacuum diode which gives four separate signals for the parts of the X-ray laser beam falling on the four quadrants of the diode. The amplitude of these four signals was equalized by shifting the position of the
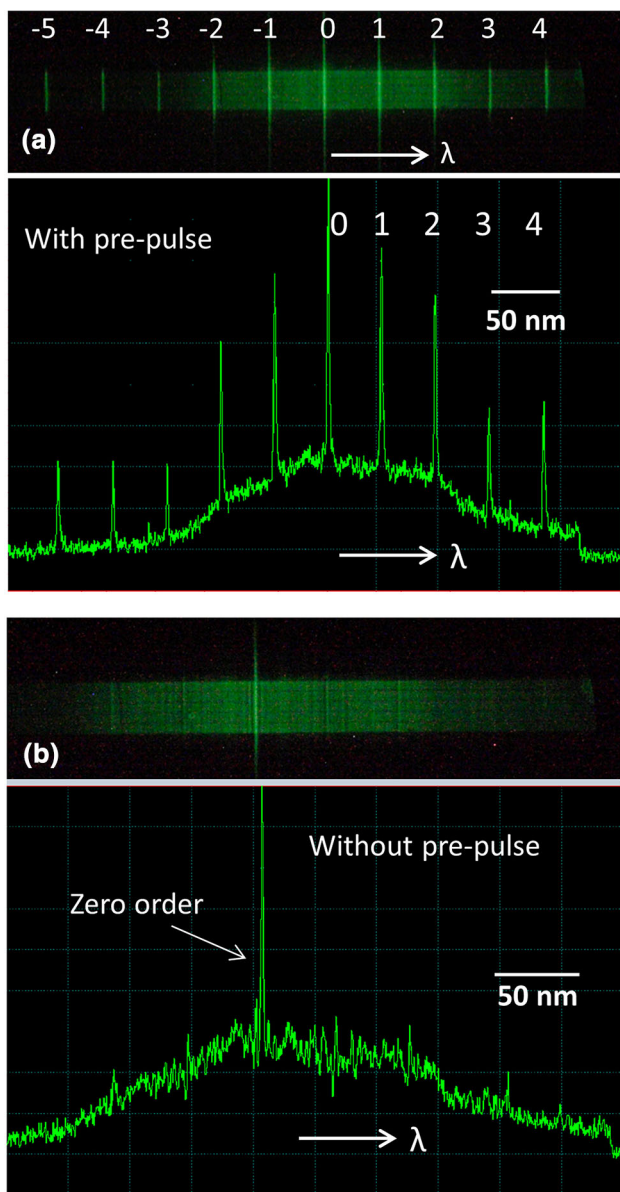
Fig. 7 Transmission grating spectrum **a** with pre-pulse, and **b** without pre-pulse. The *corresponding line* profile is shown below the spectrum

Fig. 8 Transmission grating spectrum showing up to 10th diffraction orders **a** with pre-pulse, and **b** without pre-pulse

quadrant diode with respect to laser beam position, and the center of the laser beam was located precisely. After identifying the position of the beam, the grating was placed precisely at the center of the beam. In order to do this, the center of the quadrant diode and the grating were matched in turn for this purpose by using a Canon DSLR camera placed just few cm away. Secondly, the grating is placed in a holder which is light tight but with cross holes for evacuation purposes.

The spectrum dispersed by the grating was recorded on the MCP–CCD detection system described earlier. The recorded transmissio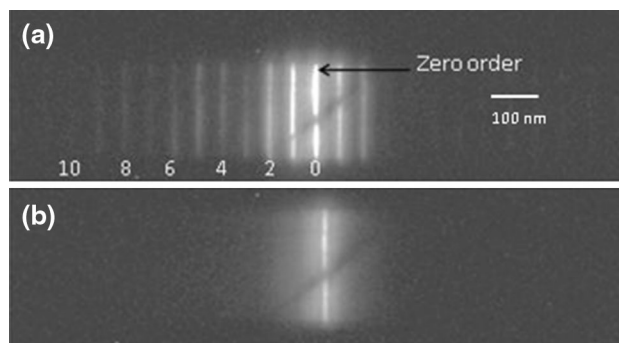n grating spectrum and its intensity profile (binned) are shown in Fig. 7a. Intense monochromatic laser line emission at 46.9 nm is distinctly observed superimposed over the continuum emission spectrum of the plasma. The separations between the observed lines are quite consistent with the various diffraction orders from the transmission grating for the lasing line at 46.9 nm. Various higher diffraction orders (up to 5th) are seen in the spectrum with prominent intensity. As in the case of spatial and temporal profiles, in this case also, all the diffraction orders of lasing line disappear in the absence of pre-pulse, as seen in Fig. 7b. The highest diffraction order observed was limited by the MCP size and the distance between the grating and MCP. When the distance between the grating and MCP was further reduced, diffraction orders as high as 10th could be seen with the X-ray laser, as shown in Fig. 8. Such high diffraction orders indicate that the X-ray laser beam is sufficiently intense.

Our detector (MCP or vacuum diode) is at a large distance (1–2 m) from the plasma source. Any radiation, which is not laser, will be much more divergent. Even if some visible and UV radiation reaches the 700 lpm transmission grating, it will be highly dispersed by a very large angle compared to the 46.9-nm laser radiation and will not be seen in the spectrum recorded by MCP. Only the XUV bremsstrahlung continuum radiation from the plasma will form a background, as seen in Fig. 7. In the vacuum diode signal, where there is no grating, the contribution from the incoherent radiation is seen as long pulse with the narrow (few ns wide) laser pulse riding on top of it (see Fig. 4). Similarly, in the recorded spatial profile of the laser beam, the incoherent radiation fills the entire MCP forming a low-intensity background and the laser spatial profile rides on top of this background. Hence, the incoherent radiation background contribution can be easily subtracted to get the laser profile.

In addition to the temporal, spatial, and spectral profiles of the X-ray laser, experiments were also carried out to study the spatial coherence of the X-ray laser beam. A
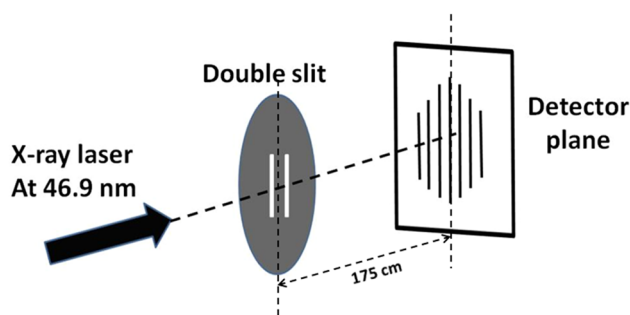
Fig. 9 A schematic diagram for coherence measurement

schematic diagram of the experimental setup for this is shown in Fig. 9. A double slit (30-μm-wide slits separated by 120 μm) was placed at a distance of 88 cm from the exit of the capillary. The wave front of the primary beam was divided equally into two parts by the double slits, which then interfere with each other to form interference fringes. The visibility of these fringes depends upon the coherence of the incident laser beam. The MCP–CCD combination was used as detector to record these fringes at a large distance (∼175 cm) from the double slit. Interference fringes with a very good contrast were successfully recorded, as shown in Fig. 10a. Figure 10b shows the line profile of the fringe pattern in a direction normal to the fringes. The measured fringe separation of ∼682 micron was found to be in good agreement with the laser wavelength at 46.9 nm. Before calculating the visibility of the fringe pattern, it is essential to remove the background from the recorded image. In order to eliminate the effect of background signal from the recorded image of the fringe pattern, two images were recorded, one with pre-pulse and the other without pre-pulse. The image without pre-pulse has only background signal (in absence of the lasing pulse) as stated earlier and also reflected in Fig. 7. Therefore, we subtracted the image without pre-pulse from the image with pre-pulse, and the resulting image provided the contribution of lasing pulse with the background eliminated. After subtracting the background due to incoherent plasma emission, the visibility of the recorded interference fringes {defined as $V = (I_{max} - I_{min})/(I_{max} + I_{min})$} was measured to be ∼85 %. For a Gaussian beam, the fringe visibility 'V' can be expressed in terms of the slit separation 'd' and the spatial coherence radius 'L_c' as $V = \exp\left(-\frac{d^2}{2L_c^2}\right)$. Using this relation between visibility and slit separation, the transverse spatial coherence length was estimated to be ∼225 μm at a distance of 88 cm from the capillary, where the double slit was placed. This measured value of the spatial coherence length is modest in comparison with what has been reported earlier for such soft X-ray lasers [43, 44] with relatively longer length of
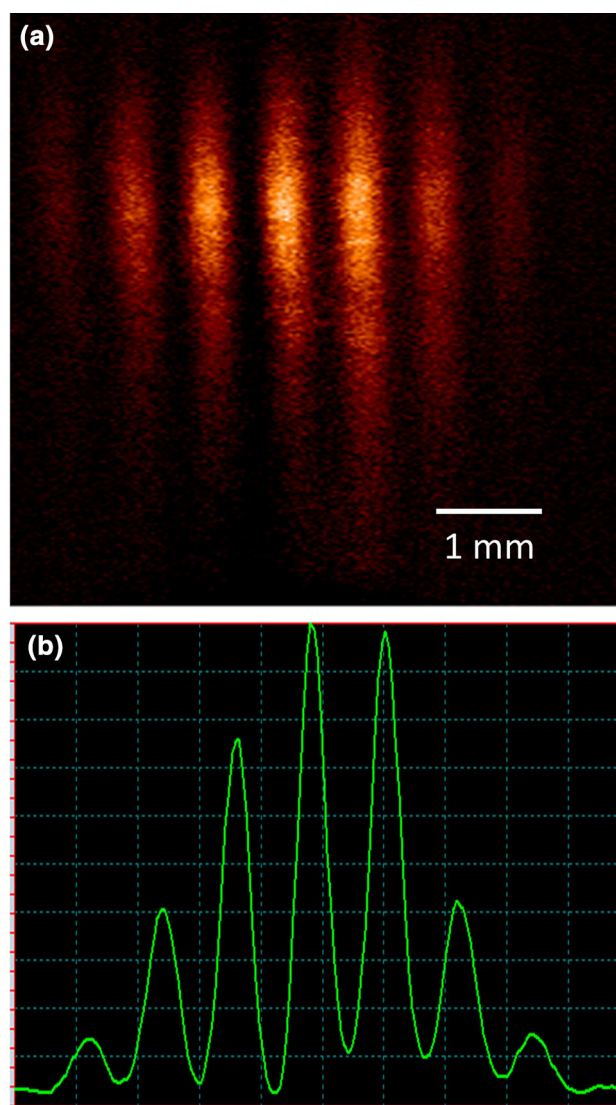

Fig. 10 a Recorded interference fringe pattern and **b** its intensity profile, in a direction normal to the fringes

capillary. This is because the spatial coherence of a discharge laser has a strong dependence on the length of the column [43, 44]. Liu et al. [44] have demonstrated full spatial coherence for a plasma column of length 36 cm.

5 Conclusion

Optimization of various parameters of capillary discharge argon plasma was carried out by monitoring the fast laser pulse recorded with vacuum photodiode. The lasing occurs only in the presence of a pre-pulse, which produces pre-plasma before the main discharge. Laser pulse width was measured to be 1.2 ns (FWHM). From the spatial profile of the X-ray laser beam, the divergence of the beam was calculated to be smaller than 3.5 mrad. The spectrum of the

lasing line at 46.9 nm was recorded using TGS. The spectrum shows higher diffraction orders as high as 10th order of the lasing line, confirming intense lasing emission at 46.9 nm. From the double slit interference, the transverse spatial coherence length of the laser beam was calculated to be ~ 225 μm at a distance of 88 cm from the capillary. Efforts are currently going on to increase the plasma column length and study its effects on various parameters such as energy, coherence length.

References

1. C.A. Brewer, F. Brizuela, P. Wachulak, D.H. Martz, W. Chao, E.H. Anderson, D.T. Attwood, A.V. Vinogradov, I.A. Artyukov, A.G. Ponomareko, V.V. Kondratenko, M.C. Marconi, J.J. Rocca, C.S. Menoni, Opt. Lett. **33**, 518 (2008)
2. P.W. Wachulak, M.C. Marconi, R.A. Bartels, C.S. Menoni, J.J. Rocca, J. Opt. Soc. Am. B **25**, 1811 (2008)
3. M.C. Marconi, P.W. Wachulak, Prog. Quantum Electron. **34**, 173 (2010)
4. M. Purvis, J. Grava, J. Filevich, M.C. Marconi, J. Dunn, S.J. Moon, V.N. Shlyaptsev, E. Jankowska, J.J. Rocca, Phys. Rev. E **76**, 046402 (2007)
5. H. Daido, Rep. Prog. Phys. **65**, 1513 (2002)
6. D.H. Martz, D. Alessi, B.M. Luther, Y. Wang, D. Kemp, M. Berrill, J.J. Rocca, Opt. Lett. **35**, 1632 (2010)
7. J. Dunn, Y. Li, A.L. Osterheld, J. Nilsen, J.R. Hunter, V.N. Shlyaptsev, Phys. Rev. Lett. **84**, 4834 (2000)
8. T. Kawachi, M. Kado, M. Tanaka, A. Sasaki, N. Hasegawa, A.V. Kilpio, S. Namba, K. Nagashima, P. Lu, K. Takahashi, H. Tang, R. Tai, M. Kishimoto, M. Koike, H. Daido, Y. Kato, Phys. Rev. A **66**, 033815 (2002)
9. Y. Wang, M.A. Larotonda, B.M. Luther, D. Alessi, M. Berrill, V.N. Shlyaptsev, J.J. Rocca, Phys. Rev. A **72**, 053807 (2005)
10. H.T. Kim, I.W. Choi, N. Hafz, J.H. Sung, T.J. Yu, K.H. Hong, T.M. Jeong, Y.C. Noh, D.K. Ko, K.A. Janulewicz, J. Tummler, P.V. Nickles, W. Sandner, J. Lee, Phys. Rev. A **77**, 023807 (2008)
11. C. Winterfeldt, C. Spielmann, G. Gerber, Rev. Mod. Phys. **80**, 117 (2008)
12. J. Feldhaus, J. Arthur, J.B. Hastings, J. Phys. B **38**, S799 (2005)
13. J.J. Rocca, Rev. Sci. Instrum. **70**, 3799 (1999)
14. J.J. Rocca, V. Shlyaptsev, F.G. Tomasel, O.D. Cortazar, D. Hartshorn, J.L.A. Chilla, Phys. Rev. Lett. **73**, 2192 (1994)
15. P. Zeitoun, G. Faivre, S. Sebban, T. Mocek, A. Hallou, M. Fajardo, D. Aubert, P. Balcou, F. Burgy, D. Douillet, S. Kazamias, G. de Lachèze-Murel, T. Lefrou, S. le Pape, P. Mercère, H. Merdji, A.S. Morlens, J.P. Rousseau, C. Valentin, Nature **431**, 426 (2004)
16. Y. Wang, E. Granados, F. Pedaci, D. Alessi, B. Luther, M. Berrill, J.J. Rocca, Nat. Photonics **2**, 94 (2008)
17. J.J. Rocca, D.P. Clark, J.L.A. Chilla, V.N. Shlyaptsev, Phys. Rev. Lett. **77**, 1476 (1996)
18. S. Heinbuch, M. Grisham, D. Martz, J.J. Rocca, Opt. Express **13**, 4050 (2005)
19. A. Ben-Kish, M. Shuker, R.A. Nemirovsky, A. Fisher, A. Ron, J.L. Schwob, Phys. Rev. Lett. **87**, 015002 (2001)
20. G. Niimi, Y. Hayashi, M. Nakajima, M. Watanabe, A. Okino, K. Horioka, E. Hotta, J. Phys. D **34**, 2123 (2001)
21. Y. Hayashi, H. Ghomi, Y. Zhao, Y. Cheng, Y. Sakai, M. Watanabe, A. Okino, K. Horioka, E. Hotta, Jpn. J. Appl. Phys. **47**, 977 (2008)
22. N. Sakamoto, M. Masnavi, M. Nakajima, T. Kawamura, K. Horioka, Jpn. J. Appl. Phys. **47**, 2250 (2008)
23. Y. Hayashi, Y. Xiao, N. Sakamoto, H. Miyahara, G. Niimi, M. Watanabe, A. Okino, K. Horioka, E. Hotta, Jpn. J. Appl. Phys. **42**, 5285 (2003)
24. Y. Hayashi, H. Taniguchi, H. Ghomi, P. Chalise, N. Sakamoto, M. Watanabe, A. Okino, M. Nakajima, K. Horioka, E. Hotta, Jpn. J. Appl. Phys. **43**, 5564 (2004)
25. G. Tomassetti, A. Ritucci, A. Reale, L. Palladino, L. Reale, S.V. Kukhlevsky, F. Flora, L. Mezi, J. Kaiser, A. Faenov, T. Pikuz, Eur. Phys. J. D **19**, 73 (2002)
26. G. Tomassetti, A. Ritucci, A. Reale, L. Palladino, L. Reale, S.V. Kukhlevsky, F. Flora, L. Mezi, A. Faenov, T. Pikuz, A. Gaudieri, Opt. Commun. **231**, 403 (2004)
27. A. Ritucci, G. Tomassetti, A. Reale, F. Flora, L. Mezi, Phys. Rev. A **70**, 023818 (2004)
28. A. Ritucci, G. Tomassetti, A. Reale, L. Reale, Appl. Phys. Lett. **86**, 101106 (2005)
29. C.A. Tan, K.H. Kwek, J. Phys. D **40**, 4787 (2007)
30. C.A. Tan, K.H. Kwek, Phys. Rev. A **75**, 043808 (2007)
31. Y. Zhao, Y. Cheng, B. Luan, Y. Wu, Q. Wang, J. Phys. D **39**, 342 (2006)
32. Y.P. Zhao, S. Jiang, Y. Xie, Q. Wang, Appl. Phys. B **99**, 535 (2010)
33. Y. Xie, Q. Wang, Y.P. Zhao, M.Z. Mo, S.T. Yang, T. Liu, D.W. Yang, Laser Phys. **20**, 226 (2010)
34. Y.P. Zhao, S. Jiang, Y. Xie, D. Yang, S. Teng, D. Chen, Q. Wang, Opt. Lett. **36**, 3458 (2011)
35. K. Kolacek, J. Schmidt, V. Bohacek, M. Ripa, O. Frolov, P. Vrba, J. Straus, V. Prukner, A.A. Rupasov, A.S. Shikanov, Plasma Phys. Rep. **34**, 162 (2008)
36. W.H. Bennett, Phys. Rev. **45**, 890 (1934)
37. M.G. Haines, Plasma Phys. Control. Fusion **53**, 093001 (2011)
38. D.D. Ryutov, M.S. Derzon, M.K. Matzen, Rev. Mod. Phys. **72**, 167 (2000)
39. V.N. Shlyaptsev, J.J. Rocca, A.L. Osterheld, Proc. SPIE Int. Soc. Opt. Eng. **2520**, 365 (1995)
40. D.E. Kim, D.S. Kim, A.L. Osterheld, J. Appl. Phys. **84**, 5862 (1998)
41. Y.B.S.R. Prasad, S. Nigam, K. Aneesh, S. Barnwal, P.K. Tripathi, P.A. Naik, C.P. Navathe, P.D. Gupta, Sadhana **36**, 349 (2011)
42. S. Nigam, K. Aneesh, C.P. Navathe, P.D. Gupta, Rev. Sci. Instrum. **82**, 024702 (2011)
43. M.C. Marconi, J.L.A. Chilla, C.H. Moreno, B.R. Benware, J.J. Rocca, Phys. Rev. Lett. **79**, 2799 (1997)
44. Y. Liu, M. Seminario, F.G. Tomasel, C. Chang, J.J. Rocca, D.T. Attwood, Phys. Rev. A **63**, 033802 (2001)